Appl. Phys. B 69, 413–416 (1999) / Digital Object Identifier (DOI) 10.1007/s003409900164

Applied Physics B
Lasers
and Optics

Quantum dot lasers: recent progress in theoretical understanding and demonstration of high-output-power operation

M. Grundmann, F. Heinrichsdorff, C. Ribbat, M.-H. Mao, D. Bimberg

Institut für Festkörperphysik, Technische Universität Berlin, Hardenbergstr. 36, D-10623 Berlin, Germany
(Fax.: +49-30/314-22569, E-mail: marius@sol.physik.tu-berlin.de)

Received: 24 June 1999/Revised version: 23 August 1999/Published online: 20 October 1999

Abstract. The field of semiconductor quantum dot (QD) diode lasers is rapidly developing. Important milestones, such as low-threshold operation and room-temperature cw operation, have been achieved in the last years. We review the progress in theoretical understanding and present recent results on high-power QD laser operation (> 3 W@1100 nm).

PACS: 85.30.V; 42.60.J; 78.55.Cr

Quantum dots (QDs) have appealed to physicists, chemists, and material engineers in the last few decades for the study of carrier confinement effects and the subsequent modification of optical properties [1]. The first realization of a QD injection laser with low-threshold current density based on self-organized QDs [2] in 1994 has newly sparked and multiplied that interest. QD lasers are now at the break-even point with conventional (quantum film) lasers regarding many properties. Low-threshold [3–5], room-temperature cw [4], high characteristic temperature ($T_0 = 385$ K between 80 K and 330 K) [6], high-temperature (214 °C [7]), and high-speed (9 GHz [8]) operation have been demonstrated [1]. The QD laser diode described in [5] exhibits the smallest threshold current density (26 A/cm^2) of any semiconductor laser diode reported so far. Applications of QD devices in systems are within reach now, also attracting more and more industrial laboratories to the field. This development will surpass the 1997 forecast [9] that active nanostructures will yield little return on investment for the next decade.

In this paper we review first the progress in the theoretical understanding of realistic QD lasers. Then we describe recent advances in QD laser devices, in particular for high-power operation.

1 Theoretical modeling of QD lasers

Theoretical interest in QDs and their modified electronic and optical properties dates back two decades [1]. Theoretical work about the application of QDs in semiconductor lasers started in the early 80s. Advances compared to quantum well lasers were predicted, such as low-threshold operation [10], high-temperature stability [11], and high modulation frequency due to large differential gain. Some of the assumptions, such as infinite barriers [11], bimolecular recombination [10], or a Fermi carrier distribution [10, 11] turn out not to describe realistic QD lasers that are available now. In the following we will discuss the correct modeling available nowadays based on the correct density of states and electronic level structure, recombination statistics, carrier distribution function, peak broadening and the resulting lasing properties.

1.1 Electronic level structure

From the QD material distribution (size, shape, and chemical composition) the electronic level structure can be deduced. It enters the modeling of QD laser properties in several ways. Most fundamentally, the level energies determine the optical transition energies and oscillator strengths and thus the emission wavelength and gain. Modeling of electronic states has been performed on many levels. Presently the most advanced methods for handling arbitrary material distributions are the eight-band $\mathbf{k} \bullet \mathbf{p}$ theory [12, 13] and the pseudopotential method [14]. The two methods give rather similar results for QDs in the 10-nm size range [12]. A comparison of eight-band $\mathbf{k} \bullet \mathbf{p}$ theory with simpler theories can be found in [12]. The precision of predictions of eight-band $\mathbf{k} \bullet \mathbf{p}$ theory is limited by the knowledge of material parameters [12] and the lack of precise information about the three-dimensional QD material distribution, although large progress has been made in the characterization of structural properties using transmission electron microscopy (TEM) [15] and cross-section scanning tunneling microscopy (XSTM) [16].

1.2 Carrier distribution

Initially one is tempted to simply assume Fermi distributions for the carriers in QDs. However, the carrier distribution function depends on the temperature [17, 18] due to

varying coupling between separate QDs. As is evident from low-temperature photoluminescence spectra, that are dominated by inhomogeneous broadening [19], QDs with different ground state energy are then equally populated – an extreme *non-equilibrium* situation. The reason is that the carrier re-emission time from a QD (in the order of several 10 ms, [20]) is much larger than the lifetime (about 1 ns, [21]). Thus different QDs can be considered as isolated systems. For a given carrier density, all dots have the same (average) population.

Only at temperatures sufficiently high that carrier re-emission can occur before recombination a Fermi distribution will be established. In that case, for a given carrier density, inversion is reached faster for large dots with the smaller ground state energy. Therefore a decreasing threshold current is expected, leading to a negative value for T_0, during the transition from the non-equilibrium to the equilibrium situation [18]. The transition regime between the two situations has been discussed for QDs with a single level in [22]. During laser operation the carrier lifetime is shortened by stimulated emission and thus a stronger tendency to non-equilibrium carrier distribution is revived.

Thermal population of wetting layer or barrier states will eventually lead to an increase of the threshold current if recombination outside the QDs takes place.

1.3 Recombination kinetics

The carrier recombination in quantum dots is of excitonic nature. When more than two carriers, for example two electrons and one hole, are present the gain becomes positive. At even higher carriers the optical recombination is due to multi-exciton complexes, leading to additional lines due to many-body phenomena. Recombination and gain at higher energies than the ground state transition evolve due to the participation of excited states. In the presence of a relaxation bottleneck, hindering carriers to reach the lowest available state before recombination, excited states play a role already at low carrier densities. A theoretical description has been given in the framework of master equations for the micro-states [23].

The gain of a quantum dot ensemble is due to many quantum dots that occupy different micro-states statistically at different times [23]. The gain−carrier density relation has been known to be linear for a long time [24]. The mono-molecular recombination process also causes the gain−current relation to be initially linear [23]. Saturation of the ground state gain with regard to carrier injection sets in, when the average carrier number per dot exceeds one exciton. A different saturation effect (known from nonlinear spectroscopy) comes into play when a high photon number in the cavity modifies the statistics by gain compression [8].

1.4 Peak broadening

There are inhomogeneous and homogeneous contributions to peak broadening. The *inhomogeneous* broadening, evident from relatively broad low-temperature photoluminescence spectra is due to the non-ideality of the ensemble with respect to fluctuations of size, shape, and composition of the QDs. Typical values are a full width at half maximum (FWHM) of 30 to 50 meV [1].

The *homogeneous* broadening is due to dephasing processes. One of them is spontaneous recombination, imposing a limit in the μeV range for typical radiative lifetimes around 1 ns [19]. Whereas at low temperatures recombination from excitons in self-organized QDs is indeed spectrally very sharp [19], phonon scattering mechanisms at room temperature lead to a homogeneous width of 7 meV as measured in [25] in a QD laser sample; this corresponds to a dephasing time of 190 fs. Under bias conditions creating inversion this time shortens to 70 fs, increasing the homogeneous broadening to 19 meV. For RT or above RT operation thus the homogeneous width comes into the range of the inhomogeneous broadening. This way the QDs become coupled via the light field, and all QDs can contribute to the gain at a specific wavelength within the ensemble.

2 High−power QD lasers

2.1 Motivation

The current lack of commercial semiconductor diode lasers for the > 1100 nm wavelength range stimulated our interest in such devices. They have important applications for pumping fiber lasers emitting in the blue spectral range based on up-conversion [26, 27]. In particular, the 480 nm transition of Tm is most efficiently pumped at 1122 nm. The realization of a laser wavelength around 1100 nm or beyond using conventional (strained) InGaAs quantum wells on GaAs is hindered by the transition from pseudomorphic, i.e. defect-free, growth to lattice-mismatch-induced dislocation formation [28] for the necessary combination of layer thickness and indium concentration. Self-organized QDs [1] are suitable to extend the wavelength range of the InGaAs/GaAs system into the infrared. The lasing wavelength can be further red-extended to at least 1300 nm [29, 30].

QDs also offer potential advantages for high-power lasers, again hardly explored, due to the zero-dimensional charge-carrier localization and reduction of charge-carrier diffusion. Reduced non-radiative surface recombination decreases facet overheating and larger catastrophic optical damage (COD) threshold is expected. These advantages can be combined with the low threshold and the high-temperature stability of QD lasers to create high-power lasers with lower temperature sensitivity and slightly larger wall-plug efficiency than conventional quantum-well-based lasers.

Here, we report on the demonstration of high-power quantum dot lasers grown by metal-organic chemical vapor deposition (MOCVD) in the 1100-nm wavelength range. Previously, operation of QD laser diodes at a maximum output power of 1 W had been reported for emission at 940 nm [31, 32] and 1.5 W at [33] for structures grown with molecular beam epitaxy. More recent results of the same group demonstrate an output power of more than 3 W at an emission wavelength of 870 nm [34].

2.2 Fabrication

We have fabricated our laser structures using MOCVD [4] on *n*-GaAs substrates. The active medium consists of three or six layers of InGaAs/GaAs QDs, respectively. The QDs

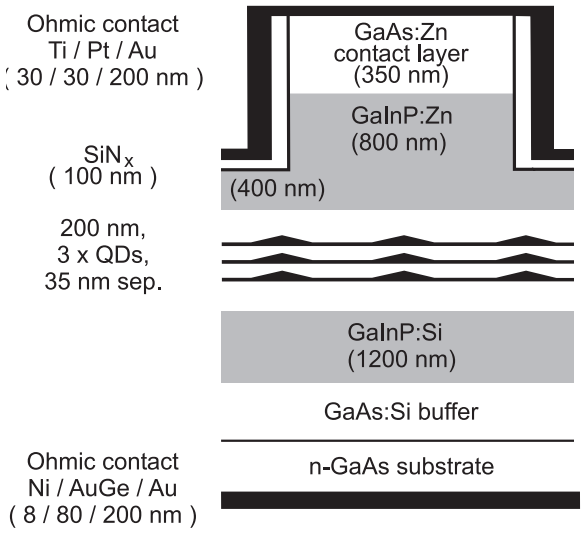

Fig. 1. Schematic structure of QD Laser

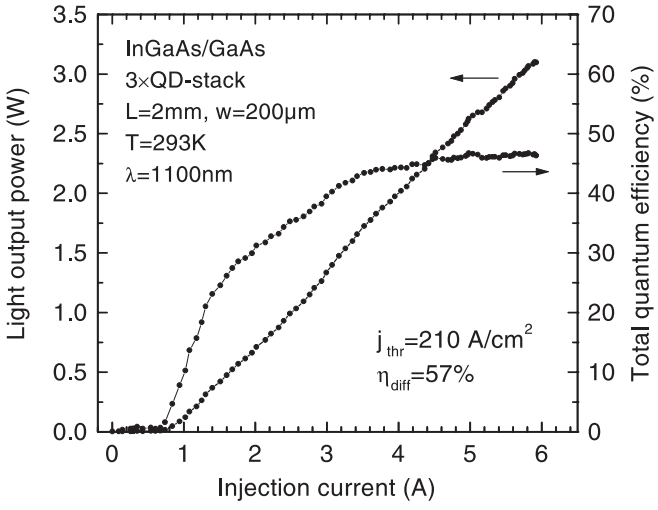

Fig. 2. Light output (front facet ×2) vs. injection current for triple-layer QD laser. Injection conditions were 650-ns pulses and a duty cycle of 1/384

have a lateral density of $(1.0-1.5)\times10^{11}\,\mathrm{cm}^{-2}$. The separation between the individual QD layers is 35(20) nm for the 3(6) layer sample, respectively; therefore the QDs are electronically decoupled. For the 20-nm barrier the QDs are vertically aligned. The QD layers are embedded in Al-free GaAs/GaInP wave-guides. Care was taken during growth of the upper waveguide, cladding and contact layers to preserve the target wavelength since growth in excess of 600 °C leads to a blueshift of the QD transition due to interdiffusion [35]. The typical inhomogeneous broadening of the photoluminescence spectrum is 84(93) meV (full width at half maximum) for the 3(6) QD layer samples, respectively.

The wafers have been processed into ridge waveguide Fabry–Pérot devices (uncoated facets) with injection stripe widths w of 50 and 200 µm. The sample structures are shown schematically in Fig. 1. The laser was mounted *p*-side up.

2.3 Device performance

In Fig. 2 the L-I curve for a $\lambda = 1100$ nm QD laser (based on 3 QD layers) is shown (cavity length $L = 2$ mm, $w = 200$ µm). The laser was driven by 650-ns pulses (duty cycle 1/384) at room temperature (293 K). A maximum peak output power of more than 3 W was achieved. The threshold current density is 210 A/cm^2 and remains at that value also after repetitive cycling the laser to 3 W. The slope efficiency is 0.62 W/A or 57%.

As can be seen from Fig. 3 the laser emission remains around 1100 nm for all input currents. This wavelength is close to the maximum of the photoluminescence spectrum (1116 nm) and therefore we conclude that the laser operates on the QD ground state. With increasing current the first mode that appeared increases in intensity. Then it saturates at an intensity of about 40 mW and more modes appear. The maximum of the spectrum switches between different longitudinal modes, most of them reaching their saturation intensity at about 40 mW per mode. The spectral full width at half maximum of the emission peak is finally 8 nm at 1.6 W and 10 nm at 3 W.

We find a vertical far-field divergence ($1/e^2$) of 104° in agreement with theoretical calculations of the vertical mode distribution expected from the cavity design. The lateral divergence is 4.5° at threshold, increasing to 9.4° at 3 W. In the laser cavity there are about 1.8×10^9 QDs, the lasing spectrum has a width of about 10 nm, about 10% of the inhomogeneous broadening. Thus at an output power of 3.5 W each QD that contributes to lasing generates about 20 nW or 10^{11} photons/s. Therefore the refill and capture time for electrons and holes can be estimated to be < 10 ps.

At a slightly shorter wavelength of $\lambda = 1068$ nm we achieved so far 4.5 W output power ($L = 1$ mm, $w = 50$ µm, six-fold QD stack) during identical pulsed operation at room temperature as above. The slope efficiency for these lasers is 0.72 W/A or 66% and the power per facet unit width is 45 mW/µm (per facet). The large power per facet width value is indicative for the advantages of QD lasers for high-power operation. The optical power density (per facet) exceeds 20 MW/cm^2.

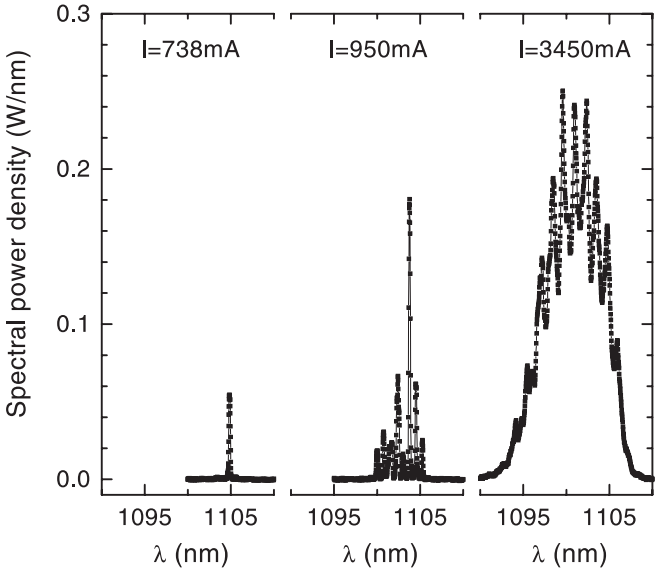

Fig. 3. Laser emission spectra for the laser from Fig. 2 at different injection currents. Spectral mode width is resolution-limited to 0.2 nm

3 Conclusion

The theoretical understanding of QD lasers has advanced tremendously together with progress in the characterization of their optoelectronic properties. Compared to quantum film lasers the modification of the density of states, the carrier distribution function, the recombination process, and the broadening mechanism impact the laser properties.

We have presented high-power quantum dot lasers grown by MOCVD. Using such QDs the emission wavelength of InGaAs on GaAs substrate was extended into the 1100-nm range. A peak power of 3(4.5) W at 1100 (1068) nm, respectively, during pulsed operation at room temperature and a slope efficiency of 57% (66%) were achieved.

Acknowledgements. Parts of this work have been funded by DFG in the framework of Sfb 296, and by BMBF within NOVALAS (Project 13N7231/7) and *Nan*Op (Competence Center for the Application of Nanostructures in Optoelectronics).

References

1. D. Bimberg, M. Grundmann, N.N. Ledentsov: *Quantum Dot Heterostructures* (Wiley, Chichester 1998)
2. N. Kirstaedter, N.N. Ledentsov, M. Grundmann, D. Bimberg, V.M. Ustinov, S.S. Ruvimov, M.V. Maximov, P. S. Kopév, Z.I. Alferov, U. Richter, P. Werner, U. Gösele, J. Heydenreich: Electron. Lett. **30**, 1416 (1994)
3. N.N. Ledentsov, V.A. Shchukin, M. Grundmann, N. Kirstaedter, J. Böhrer, O. Schmidt, D. Bimberg, V.M. Ustinov, A.Yu. Egorov, A.E. Zhukov, P.S. Kopév, S.V. Zaitsev, N.Y. Gordeev, Z.I. Alferov, A.I. Borovkov, A.O. Kosogov, S.S. Ruvimov, P. Werner, U. Gösele, J. Heydenreich: Phys. Rev. B **54**, 8743 (1996)
4. F. Heinrichsdorff, M.-H. Mao, N. Kirstaedter, A. Krost, D. Bimberg, A.O. Kosogov, P. Werner: Appl. Phys. Lett. **71**, 22 (1997)
5. G.T. Liu, A. Stintz, H. Li, K.J. Malloy, L.F. Lester: 1999 Digest of the IEEE LEOS Summer Topical Meetings, IEEE Catalog #99TH8455, ISBN: 0-7803-5633-0, p. 19
6. M.V. Maximov, N.Y. Gordeev, S.V. Zaitsev, P.S. Kopév, I.V. Kochnev, N.N. Ledentsov, A.V. Lunev, S.S. Ruvimov, A.V. Sakharov, A.F. Tsatsul'nikov, Y.M. Shernyakov, Z.I. Alferov, D. Bimberg: Semiconductors **31**, 124 (1997)
7. F. Schäfer, J.P. Reithmaier, A. Forchel: Appl. Phys. Lett. **74**, 2915 (1999)
8. D. Bimberg, N. Kirstaedter, N.N. Ledentsov, Z.I. Alferov, P.S. Kopév, V.M. Ustinov: IEEE J. Sel. Top. Quantum Electron. **3**, 1 (1997)
9. R.S. Williams: Functional Nanostructures, Proc. Workshop of the World Technology Evaluation Center (WTEC) on R&D Status and Trends in Nanoparticles, Nanostructured Materials, and Nanodevices in the US (1997), http: //itri.loyola.edu/nano/us_r_n_d/toc.htm
10. M. Asada, A. Kameyama, Y. Suematsu: IEEE J. Quantum Electron. **QE-20**, 745 (1984)
11. Y. Arakawa, H. Sakaki: Appl. Phys. Lett. **40**, 939 (1982)
12. O. Stier, M. Grundmann, D. Bimberg: Phys. Rev. B **59**, 5688 (1999)
13. H. Jiang, J. Singh: IEEE J. Quantum Electron. **QE-34**, 1188 (1998)
14. A. Zunger: MRS Bulletin **23**, 35 (1998)
15. S. Ruvimov, P. Werner, K. Scheerschmidt, J. Heydenreich, U. Richter, N.N. Ledentsov, M. Grundmann, D. Bimberg, V.M. Ustinov, A.Y. Egorov, P.S. Kopév, Z.I. Alferov: Phys. Rev. B **51**, 14766 (1995); S. Ruvimov, K. Scheerschmidt: Phys. Status Solidi A **150**, 471 (1995)
16. H. Eisele, O. Flebbe, T. Kalka, C. Preinesberger, F. Heinrichsdorff, A. Krost, D. Bimberg, M. Dähne-Prietsch: Appl. Phys. Lett. **75**, 106 (1999)
17. L.V. Asryan, R.A. Suris: Semicond. Sci. Technol. **11**, 1 (1996)
18. M. Grundmann, D. Bimberg: Jpn. J. Appl. Phys. **36**, 4181 (1997)
19. M. Grundmann, J. Christen, N.N. Ledentsov, J. Böhrer, D. Bimberg, S.S. Ruvimov, P. Werner, U. Richter, U. Gösele, J. Heydenreich, V.M. Ustinov, A.Y. Egorov, A.E. Zhukov, P.S. Kopév, Z.I. Alferov: Phys. Rev. Lett. **74**, 4043 (1995)
20. C.M.A. Kapteyn, F. Heinrichsdorff, O. Stier, M. Grundmann, D. Bimberg: Proc. 24th International Conference on The Physics of Semiconductors (ICPS-24), Jerusalem, Israel, ed. by D. Gershoni (World Scientific, Singapore)
21. R. Heitz, M. Veit, N.N. Ledentsov, A. Hoffmann, D. Bimberg, V.M. Ustinov, P. S. Kopév, Z.I. Alferov: Phys. Rev. B **56**, 10435 (1997)
22. H. Jiang, J. Singh: Appl. Phys. Lett. **85**, 7438 (1999)
23. M. Grundmann, D. Bimberg: Phys. Rev. B **55**, 9740 (1997)
24. K.J. Vahala: IEEE J. Quantum Electron. **QE-24**, 523 (1988)
25. P. Borri, W. Langbein, J. Hvam, F. Heinrichsdorff, M.-H. Mao, D. Bimberg: Phys. Rev. B **60**, 7784 (1999)
26. H. Zellmer, S. Buteau, A. Tünnermann, H. Welling: Electron. Lett. **33**, 1383 (1997)
27. H. Zellmer, K. Plamann, G. Huber, H. Scheife A. Tünnermann: Electron. Lett. **34**, 565 (1998)
28. M. Grundmann, D. Bimberg, A. Fischer-Colbrie, J.N. Miller: Phys. Rev. B **41**, 10120 (1990)
29. G. Park, D.L. Huffaker, Z. Zou, O.B. Shchekin, D.G. Deppe: IEEE Photon. Technol. Lett. **11**, 301 (1999)
30. Y.M. Shernyakov, D.A. Bedarev, E.Y. Kondratéva, P.S. Kopév, A.R. Kovsh, N.A. Maleev, M.V. Maximov, S.S. Mikhrin, A.F. Tsatsul'nikov, V.M. Ustinov, B.V. Volovik, A.E. Zhukov, Z.I. Alferov, N.N. Ledentsov, D. Bimberg: Electr. Lett. **35**, 898 (1999)
31. Y.M. Shernyakov, A.Y. Egorov, A.E. Zhukov, A.V. Zaitsev, A.R. Kovsh, I.L. Krestnikov, A.V. Lunev, N.N. Ledentsov, M.V. Maximov, A.V. Sakharov, V.M. Ustinov, Z. Zhen, P.S. Kopév, Z.I. Alferov, D. Bimberg: Tech. Phys. Lett. **23**, 149 (1997)
32. M.V. Maximov, Y.M. Shernyakov, A.F. Tsatsul'nikov, A.V. Lunev, A.V. Sakharov, V.M. Ustinov, A.Y. Egorov, A.E. Zhukov, A.R. Kovsh, P.S. Kopév, L.V. Asryan, Z.I. Alferov, N.N. Ledentsov, D. Bimberg, A.O. Kosogov, P. Werner: J. Appl. Phys. **83**, 5561 (1998)
33. Y.M. Shernyakov, A.Y. Egorov, B.V. Volovik, A.E. Zhukov, A.R. Kovsh, A.V. Lunev, N.N. Ledentsov, M.V. Maximov, A.V. Sakharov, V.M. Ustinov, Z. Zhao, P.S. Kopév, Z.I. Alferov, D. Bimberg: Tech. Phys. Lett. **24**, 351 (1998)
34. A.R. Kovsh, D.A. Livshits, A.E. Zhukov, A.Yu. Egorov, M.V. Maximov, V.M. Ustinov, I.S. Tarasov, N.N. Ledentsov, P.S.Kopév, Z.I. Alferov, D. Bimberg: Pis'ma v JTP **25**(11), 41 (1999), (Phys. Tech. Lett. **25**, 438 (1999))
35. F. Heinrichsdorff, M. Grundmann, O. Stier, A. Krost, D. Bimberg: J. Crystal Growth **195**, 540 (1998)